Indian Geotech J (August 2024) 54(4):1482–1499
https://doi.org/10.1007/s40098-023-00826-0

ORIGINAL PAPER

FEM-SRT-Based Slope Analysis Considering Different Geometric Shapes and Loading Conditions

Guru Das[1] · Avijit Burman[1]

Received: 8 March 2023 / Accepted: 21 November 2023 / Published online: 19 December 2023

Abstract Among various available methods for slope analysis, the limit equilibrium method is very popular because of its simple concepts. The limit analysis method and the finite element method (FEM) also can perform stability analysis of a slope. Increasing computing power and the easy accessibility of inexpensive numerical modeling codes have made the finite element method a very attractive tool for the practical assessment of slope stability. The present study reports the results of slope stability analysis of a few problems analyzed using a developed program utilizing FEM. This program employs a strength reduction technique based on FEM. Mohr–Coulomb strength criterion of soil is used for predicting the stress state, while the viscoplastic algorithm is used for stress redistribution. Non-convergence of the algorithm to achieve the desired equilibrium of all forces in the system is adopted as a marker of slope failure. Further, to put the proposed method to the test, a few examples from the literature are analyzed using the developed program. The example problems cover a homogenous slope with water loading, an inclined layered slope, and a staged embankment subjected to different forms of loading including earthquake forces, pore water pressure, external water pressure, etc. The results of each analysis are compared with other researchers work, and it is found that the obtained results are in good agreement. Deformed mesh, equivalent viscoplastic strain contour plots, and failure function contour plots are used for illustrating the failure state.

✉ Avijit Burman
avijitburman@yahoo.com

Guru Das
gurud.ph21.ce@nitp.ac.in

[1] Department of Civil Engineering, National Institute of Technology , Patna, Bihar, India

Keywords Slope stability analysis · Finite element method · Strength reduction technique · Mohr–Coulomb failure criterion

Introduction

In various geotechnical structures such as natural slopes, highways, dams, open pit mines, analysis of slope stability is an essential requirement. As a result, the topic of slope analysis has attracted a growing amount of interest from geotechnical researchers [1]. Decades of effort have been devoted to predicting the extent of a slope's stability and preventing its catastrophic collapse. Current slope analysis techniques can be categorized into three groups: limit equilibrium method (LEM), limit analysis method (LAM), and finite element method (FEM). Due to its ease of use [2], LEM is the most widely used approach; however, its solution is deemed imprecise as a result of idealized mechanical assumptions regarding the pre-defined failure shape of the slope. The incapability of LEM to ascertain the evolution path of the failure zone of a slope is regarded as a significant shortcoming of the method. Moreover, LAM has played an increasingly crucial role in slope stability analysis. Drucker & Prager [3] carried out the first LAM-based slope stability analysis. LAM offers a simplified calculation procedure and strict bounds for limit state solutions, thereby broadening the scope of slope stability applications [4–6]. The upper bound theorem-based solution is derived from a velocity domain that is kinematically admissible and satisfies the velocity boundary conditions [7]. The lower bound theorem-based solution is derived from a stress domain that is statically admissible, satisfies the stress boundary conditions as well as equilibrium, and violates the yield condition nowhere [8]. If the two solutions coincide, the method yields the correct

solution to the problem under consideration [9]. Moreover, implementing the definition of the upper or lower bound theorem in terms of dealing with complex slope configurations and irregular soil deposition problems is challenging, and this limitation poses specific obstacles to its widespread application. As an alternative to LEM and LAM, FEM has evolved as a robust and exhaustive method for handling slope stability analysis. After assigning a realistic stress–strain constitutive model to the soil material, FEM has the potential to compute expected slope deformations and the development of the plastic zone with no requirement for prior assumptions. In addition, FEM is well-prepared to deal with loading sequences and complex slope geometry commonly observed in geotechnical engineering, which are major challenges for the LEM and LAM. Thus, the FEM appears to be a more credible and versatile technique for modeling and assessing the stability of a slope.

Conventional procedures to perform stability analysis consist of two simultaneous activities: figuring out the factor of safety (F_S) and identifying the critical failure surface (CFS). Zienkiewicz et al. [10] initially proposed the strength reduction technique (SRT). SRT has garnered considerable interest from the research community in general. Given its utility and dependability in the determination of the state of slope approaching instability, SRT has made significant progress. FEM in conjunction with SRT has moved to the forefront of geotechnical engineering practice because of its capability to model progressive failure mechanism and eventually identify the limiting condition. FEM-SRT has been equipped with an interesting trait of determining a unique value of F_S with spontaneous identification of zones which are unable to sustain the outstanding stresses. Numerous literature utilizing the FEM-SRT for stability analysis has been presented in recent years.

Griffiths and Lane [11] used FEM-SRT for analyzing stability of slope under different loading conditions. Chugh [12] discussed about the commonly used boundary conditions in slope stability analysis. Cheng et al. [13] compared FEM-SRT with the LEM and found that two methods are in good agreement. Berilgen [14] investigated stability of slopes under rapid drawdown using FEM-SRT. Zheng et al. [15] used maximum equivalent plastic strain as a tool to determine critical slip surface using FEM-SRT. Khosravi et al. [16] investigated stability of seismically loaded slopes using FEM-SRT. Lu et al. [17] used FEM-SRT to perform stability analysis of slopes with groundwater during earthquakes. Chen et al. [18] recommended that, with regard to computing expense, a two-grid approach is preferable. Tschuchnigg et al. [19] provided solution for overcoming the numerical instabilities associated with the LEM and FEM. Dyson and Tolooiyan [20] proposed novel search strategies to minimize calculation times for determination of factor of safety using strength reduction technique (SRT). Meng et al. [21] proposed a new procedure of slope stability analysis involving heterogeneous geomaterials. Liu [22] proposed a new strength reduction-based method to overcome the abnormalities of large analysis errors and low analysis efficiency associated with existing methods. Sun et al. [23] used residual displacement increment criterion as an indication of slope failure using the SRT. Mebrahtu et al. [24] used SRT for the slope stability assessment of the landslide prone hills in Debre Sina area, Ethiopia.

Despite the presence of a lot of literary works on the subject of slope analysis using traditional limit equilibrium method, very little amount of literary works is found using the finite element strength reduction technique for performing slope stability analysis. There are few accounts of the study of the stability of the slopes subjected to seismic loading, pore water pressure, and reservoir loading using FEM-SRT despite its capabilities to determine the failure zones spontaneously. Stability analysis of stepped soil slope and stepped soil slope subjected to seismic loading in horizontal and vertical directions using FEM-SRT is also rarely studied. In this study, the development procedure of a software program for performing stability analysis of soil slope using FEM-SRT method is discussed. The program incorporates a failure criterion along with the provision of pictorial outputs for mapping the failure mechanism of the soil slope. Further, the ideas adopted for the creation of FEM program for performing stability analysis of seismically loaded slopes are also discussed. In addition to reservoir loading, the discussion of the concept underlying the formulation of a program for stability analysis of submerged slopes is illustrated. The procedure for incorporating pore pressure loading during FEM simulation of slope failure is also discussed. A slope problem with interspaced weak layer between two soil layers with stronger material properties has been also analyzed. A staged embankment is analyzed using the current program to assess its applicability in case of slopes with berm. Graphical output consists of deformed mesh, equivalent viscoplastic strain contour plot, and failure function contour plot for the slope domain. Deformed mesh is used as a tool to ascertain the failure mechanism developed and check for the existence of conflicting failure mechanism. Equivalent viscoplastic strain contour plot is used as a tool to illustrate the zone experiencing severe strains. The plot of failure function demonstrates the non-uniform distribution of stresses at the state of yield. In addition to the desired F_S value of the slope, FEM-based analysis yields information about the displacements and stress conditions at the failure state. To put the proposed software program to test, few exemplar slope stability problems have been taken from recent literary works. All analyzed results were compared to the findings of other researchers. The authors feel that the present paper will contribute toward popularizing the FEM-based

slope analysis techniques among the practicing engineers and research community as well.

Methodology

The paper discusses the development finite element program for performing various slope analysis problems. The finite element program employs 2D plane strain analysis and Mohr–Coulomb failure criteria for representing the stress–strain behavior of soil. The viscoplastic algorithm is used to induce failure in the slope by progressively redistributing the stresses inside the soil mass. The program can also simulate the effects of earthquakes using a pseudo-static seismic coefficient, as well as the effects of varying water levels and pore water pressure. It uses eight-nodded quadrilateral elements with reduced numerical integration for generating gravity loads, making stiffness matrices, estimating pore water pressure, and redistributing stresses.

Material Model

The Mohr–Coulomb elastoviscoplastic material model used in the current slope stability software program takes as an input six soil properties, namely angle of internal friction (ϕ'), cohesion (c'), dilation angle (ψ), unit weight of soil (γ), Young's modulus of elasticity (E) and Poisson's ratio (ν). As with any conventional slope stability analysis procedure, c', ϕ' and γ are the most important parameters in the FEM-based slope stability analysis. The dilation angle (ψ) governs the soil's volume change during yielding. Since slope stability analysis is generally unconstrained, the selection of ψ is less significant. As accurate prediction of slope safety factors is the primary goal of the current study, an acceptable value of ψ equal to zero is adopted. Since zero volume change during the yield and non-associated flow rule is made use of. Assuming tension positive and compression negative, the Mohr–Coulomb failure criterion f_{mc} in terms of principal stresses $\left(\sigma_1', \sigma_3'\right)$, effective angle of internal friction (ϕ'°), and effective cohesion (c') is given by Eq. 1. For the slope domain, the stress state can be predicted either to be elastic when $f_{\mathrm{mc}} < 0.0$ or yielding in case $f_{\mathrm{mc}} \geq 0.0$.

$$f_{\mathrm{mc}} = \left(\sigma_1' + \sigma_3'\right)\sin\phi' - \left(\sigma_1' - \sigma_3'\right) - 2c'\cos\phi' \tag{1}$$

It has been observed that the elastic constants E and ν have substantial effect on the deformations calculated before the soil slope achieves the state of failure, but calculated value of factor of safety (F_S) is found to be absolutely independent[11]. For soils, E can be determined using 1-D consolidation test as a function of compressibility response. For current study, a nominal value of E=10^5 kPa is assumed. Poisson's ratio ν is generally found to lie between 0.20 and 0.50. For the current study, a nominal value of $\nu = 0.30$ is assumed.

Strength Reduction Technique (SRT)

With time, the SRT becomes an established method for assessing slope stability, not only in academic research but also in analysis of real-world geotechnical problems. Its dominance is due to its following benefits:

1. The SRT is suitable for complex soil slope geometries subjected to complex loading and diverse boundary conditions.
2. No prior assumptions must therefore be made regarding the CFS. The failure occurs spontaneously in soil zones where shear strength is insufficient to withstand the generated shear stresses.
3. Since SRT is coupled with displacement-based FEM, it is possible to obtain details regarding displacements, normal strains, and shear strains as well as normal and shear stresses. These parameters can be obtained corresponding to any underlying stress state from initial to failure.

In the strength reduction method, strength parameters of the soil are reduced using a suitable factor (SRF) that brings the slope to the limiting state of failure. The reduced Mohr–Coulomb shear strength parameters are written as follows:

$$c^r = \frac{c'}{\mathrm{SRF}} \tag{2}$$

$$\phi^r = \tan^{-1}\left(\frac{\tan\phi'}{\mathrm{SRF}}\right) \tag{3}$$

Viscoplastic Algorithm

In SRT-based slope analysis, failure is induced by progressively factoring the shear strength parameters of soil. The strategy of reduction in strength parameters of the soil to obtain a failure state can be implemented by using viscoplastic algorithm that adjusts the induced load on the system in an incremental manner. Assuming the material is yielding, the strain increment $\mathbf{\Delta\varepsilon^{itr}}$ will contain both elastic $\mathbf{\Delta\varepsilon_{el}^{itr}}$ and viscoplastic component $\mathbf{\Delta\varepsilon_{vp}^{itr}}$.

$$\mathbf{\Delta\varepsilon^{itr}} = \mathbf{\Delta\varepsilon_{el}^{itr}} + \mathbf{\Delta\varepsilon_{vp}^{itr}} \tag{4}$$

Stress increments $\mathbf{\Delta\sigma^{itr}}$ are calculated as per Eq. 5 where $\mathbf{D^e}$ represents the elastic constitutive matrix.

$$\Delta\sigma^{itr} = D^{e}\Delta\varepsilon_{el}^{itr} \tag{5}$$

The increment in stress components $\Delta\sigma^{itr}$ is added to calculated stresses from the earlier load step, and the modified stresses are substituted into the Mohr–Coulomb failure criterion. If the stresses calculated are such that there is a need for redistribution, the load vector F^{itr} is modified. This load vector F^{itr} holds two types of loads as given by Eq. 6 where F_{ext}^{itr} is the external gravity load increment and F_{int}^{itr} is the internal loads vector that changes from one plastic iteration to another.

$$F^{itr} = F_{ext}^{itr} + F_{int}^{itr} \tag{6}$$

The body load vector for the next iteration is calculated by summing the integral for all elements which consists of a yielding gauss point as per Eq. 7.

$$F_{int}^{itr+1} = F_{int}^{itr} + \sum_{1}^{no.of elements} \iint B^{T}D^{e}\delta\varepsilon_{vp}^{itr}\,dxdy \tag{7}$$

The viscoplastic strain increment $\delta\varepsilon_{vp}^{itr}$ is calculated as the product of viscoplastic strain rate $\dot{\varepsilon}_{vp}^{itr}$ and time step Δt where $\dot{\varepsilon}_{vp}^{itr}$ is calculated using the flow rule as shown in Eq. 8. Here, λ is the plastic multiplier considered equal to yield function f_{mc} and Q is the plastic potential function.

$$\dot{\varepsilon}_{vp}^{itr} = \lambda\frac{\partial Q}{\partial\sigma} \tag{8}$$

The detailed procedure of estimating $\dot{\varepsilon}_{vp}^{itr}$ has been discussed by many eminent researchers [10, 25].

Integration Procedure

Numerical integration using Gauss quadrature rules known as Gaussian product rules is used as the procedure for the solution of integral equations. For the current study, reduced 2×2 integration strategy is used. The body load vector for the next iteration is calculated as shown below:

$$F_{int}^{itr+1} = F_{int}^{itr} + \sum_{1}^{no.of elements} \int_{-1}^{+1}\int_{-1}^{+1} B^{T}D^{e}\delta\varepsilon_{vp}^{itr}\,detJ\,d\xi d\eta \tag{9}$$

$$F_{int}^{itr+1} = F_{int}^{itr} + \sum_{1}^{no.of elements} \sum_{i}\sum_{j} W_{i}W_{j}B^{T}D^{e}\delta\varepsilon_{vp}^{itr}\,detJ \tag{10}$$

where det J stands for the determinant of Jacobian matrix used for the transformation from the global coordinate system to the local coordinate system. Since four integration points i.e., 2×2 Gaussian quadrature are made use of, therefore i and j vary from 1 to 2. W_i and W_j are the weight factors and other parameters have their usual meanings.

Slope Failure Mechanism

Failure of slopes occurs when driving forces outweigh resisting forces. The driving force is typically gravity, and the opposing force is the shear strength of the slope material. This basically forms the classical definition used in the case of conventional slope stability analyses. In the slope analysis using FEM, the soil mass is represented as a continuum, and failure is progressive in the sense that the inelastic region expands as the load increases. Between the initial yield state and the final failure state, a wide range of loading can exist. Based on the definition of failure, any value within this range may represent the critical load. A few of the most commonly utilized failure criteria such as bulging of slope line [26], limit shear [27], and non-convergence [28] have been used earlier. Bulging of the slope line means specifying a maximum tolerable limit for horizontal displacements along the surface of the slope. Limit shear consists of limiting the shear stresses on the potential failure surface.

For the current study, non-convergence is adopted as the failure definition since this is the most reasonable criterion to employ when solving force equilibrium equations using an iterative procedure. An assessment of convergence is performed inside the viscoplastic iteration loop. This assessment uses the nodal displacement for the current iteration U^{itr}, the nodal displacement from the previous iteration U^{itr-1}, the maximum nodal displacement for the current iteration U_{max}^{itr}, and convergence tolerance *ctol*. The convergence assessment is given by:

$$\frac{\left|U^{itr} - U^{itr-1}\right|}{\left|U_{max}^{itr}\right|} < ctol \tag{11}$$

If the convergence assessment as per Eq. 11 is set to false within the plastic iteration limit specified, it implies the incapability of the algorithm to simultaneously establish global equilibrium along with the fulfilment of the Mohr–Coulomb failure criterion. If the algorithm cannot meet these requirements, the slope is deemed to have failed. Simultaneous slope failure and numerical non-convergence are accompanied by an upsurge in the mesh's nodal displacements. For the current study, the maximum number of iterations is limited to 1000.

Iteration Scheme

For slope stability analysis using the FEM-SRT method, an iterative procedure is used to determine the smallest value

of SRF for which the viscoplastic stress redistribution algorithm fails to converge. Each iteration step consists of four rigorous computational procedures, i.e., global analysis to determine global nodal displacements, local analysis for determining stresses, strains, and yield function values, updating the global load vector, and finally convergence check. The algorithm of the iteration strategy for obtaining the SRF value is shown in Table 1.

Automatic Search for SRF

The limiting state of failure of the slope is searched through the application of SRT. Usually, multiple iterations are necessary to reach the final value of SRF, which also represents the factor of safety (F_S) of the slope against failure. Using bracketing and bisection, it is possible to find the successive trial values of SRF if the collapse is not initiated at the current stage. Initially, upper and lower brackets are created. Any trial value of SRF at which a simulation converges represents the initial lower bracket $\left(\mathrm{SRF}_{\mathrm{low}}\right)$. The initial upper bracket consists of any trial value of SRF for which the simulation fails to converge $\left(\mathrm{SRF}_{\mathrm{upp}}\right)$. Then, a point in the middle of the upper and lower brackets is examined as per Eq. 12.

$$\mathrm{SRF} = \frac{\mathrm{SRF}_{\mathrm{low}} + \mathrm{SRF}_{\mathrm{upp}}}{2} \tag{12}$$

If the simulation converges, this value is substituted for the lower bracket. Whenever the simulation fails to converge, the upper bracket is changed. The procedure is repeated until the gap between the upper and lower brackets falls below a predetermined tolerance.

As per Soranzo et al. [29], the safety factor rarely exceeds 10. Therefore, the value of $\mathrm{SRF}_{\mathrm{low}}$ is such that it should not be less than zero and $\mathrm{SRF}_{\mathrm{upp}}$ should not be greater than 10. The number of iterations n_{f} and prescribed tolerance $\mathrm{tol}_{\mathrm{f}}$ are related to each other as per Eq. 13 [30].

$$n_{\mathrm{f}} \geq \frac{\log\left(\frac{\mathrm{SRF}_{\mathrm{upp}}^{\mathrm{ini}} - \mathrm{SRF}_{\mathrm{low}}^{\mathrm{ini}}}{\mathrm{tol}_{\mathrm{f}}}\right)}{\log 2} \tag{13}$$

Using Eq. 13 for $\mathrm{SRF}_{\mathrm{upp}}^{\mathrm{ini}} = 10$, $\mathrm{SRF}_{\mathrm{low}}^{\mathrm{ini}} = 0$, and a convergence $\mathrm{tol}_{\mathrm{f}} = 0.02$, it is found that n_f should be greater than or equal to 10. As per the study of Tanakan [31], it is found that the bisection method is suitable for giving correct results up to three digits for n_{f} approximately equal to 20. So, for the current case, $n_{\mathrm{f}} = 20$ is adopted for automatic search of SRF.

Table 1 Algorithm for the iteration strategy for calculating SRF

For each SRF ***do***
- Evaluate reduced shear strength parameters
- For each iteration step ***do***
  - Update global load vector $\mathbf{F}^{\mathbf{itr}}$
  - Solve for global nodal displacements $\mathbf{U}^{\mathbf{itr}}$
  - Check displacement convergence $\frac{\left|\mathbf{U}^{\mathbf{itr}} - \mathbf{U}^{\mathbf{itr\text{-}1}}\right|}{\left|\mathbf{U}_{\mathbf{max}}^{\mathbf{itr}}\right|} < ctol$
  - For each element ***do***
    - Extract local nodal displacements $\mathbf{u}_{\mathbf{iel}}^{\mathbf{itr}}$
    - For each integration point ***do***
      - Evaluate strain displacement matrix $\mathbf{B}$
      - Evaluate stress increment $\boldsymbol{\Delta\sigma}^{\mathbf{itr}}$, strain increment $\boldsymbol{\Delta\varepsilon}^{\mathbf{itr}}$
      - Evaluate yield function f_{mc}
      - Check if the yield function is greater than or less than zero
      - If the yield function value is greater than zero, evaluate the body load vector
    - ***End do***
    - Evaluate element body load vector $\mathbf{F}_{\mathbf{intiel}}^{\mathbf{itr}}$
  - ***End do***
- ***End do***

End do

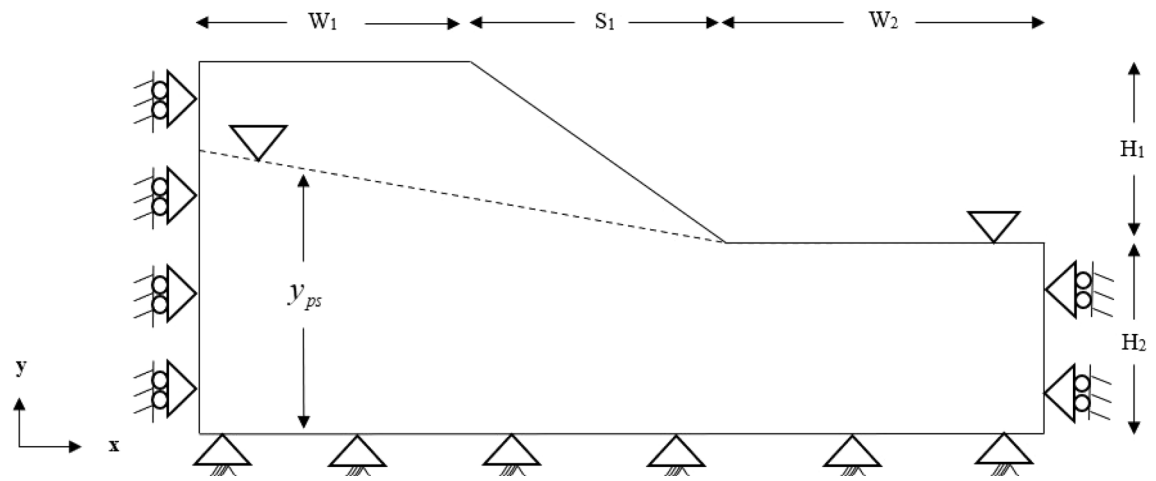

Fig. 1 Schematic diagram and the boundary conditions for a 2-D soil slope

Displacement Boundary Conditions

For accurate FEM modeling, it is necessary to specify appropriate boundary conditions for the discretized slope domain. The boundary conditions of an illustrative slope domain are depicted in Fig. 1. Along the base of the considered domain, vertical and horizontal displacements are restricted. Along the left and right boundaries, rollers are attached allowing only vertical displacements. It is well known that slope stability analysis is a boundary value problem. For the solution of boundary value problems, usually roller and fixed boundary conditions are used for solid mechanics problems. For the current slope stability model, boundary conditions are defined using rollers as side supports, and the nodes at the bottom boundary are pinned/fixed. Similar boundary conditions were also used by Griffiths and Lane [11] while analyzing slope stability problems using finite element method. The specifications of the roller or pinned support conditions are only made for the exterior boundary of the slope domain. In order to capture the failure mechanism of the sloping portion, the exterior boundary should be considered far away from the failure zones, so that undesirable end effects can be avoided. In the present work, all specifications of boundary conditions have been made keeping in mind the above-mentioned considerations.

Effect of Earthquake

Earthquakes cause horizontal and vertical accelerations of slopes, causing cyclic fluctuations in stresses within the slope, generally above their static values for a brief duration. This smaller duration may not affect the strength of soil but may lead to instability when dynamic loads act in opposite directions. The pseudo-static approach is one of the first seismic stability study procedures, in which the earthquake loading is modeled by an equivalent static force equal to the weight of the soil multiplied by a pseudo-static seismic coefficient acting in horizontal or vertical directions, i.e., k_h or k_v. The seismic force is modeled by modifying the nodal gravity load vector for each eight-nodded isoparametric element by adding or subtracting the product of the pseudo-static seismic coefficient and the load acting on the ith node along x and y directions, respectively.

$$f_{2i-1} = f_{2i-1} \pm k_h \times f_{2i-1} \tag{14}$$

$$f_{2i} = f_{2i} \pm k_v \times f_{2i} \tag{15}$$

Effect of Pore Water Pressure

In the case of limit equilibrium-based slope stability analysis, pore water pressure at a point is computed as the product of the unit weight of water (γ_w) and the height of that point below the piezometric surface (h). Pore water pressure inside the soil is computed at the element Gauss points lying below the piezometric surface following the same idea as in the case of the limit equilibrium method. The procedure to consider the effect of pore water pressure in the computer program is described in the forthcoming paragraph.

Using the coordinates of the points through which the phreatic surface passes, a curve of the form $y = f(x)$ is defined to connect these points. For each element, the global coordinates of Gauss points x_{ig}^{ele} and y_{ig}^{ele} are calculated as the summation of the product of the shape function N_i corresponding to each node of the element and the global nodal coordinates of the associated nodes.

$$x_{ig}^{ele} = \sum_{i=1}^{n} N_i x_i \tag{16}$$

$$y_{ig}^{ele} = \sum_{i=1}^{n} N_i y_i \tag{17}$$

Thereafter, control statements are used to ascertain if the calculated global vertical coordinates lie below the phreatic surface or not. Corresponding to each value of x_{ig}^{ele}, the function defining the phreatic surface curve is used to calculate the phreatic surface vertical coordinate y_{ps}. If the calculated value of y_{ig}^{ele} is found to be located below y_{ps}, then pore water pressure pwp_{ig}^{ele} is calculated as the product of the unit weight of water γ_w and the difference of y_{ps} and y_{ig}^{ele}.

$$pwp_{ig}^{ele} = \gamma_w \times \left(y_{ps} - y_{ig}^{ele}\right) \tag{18}$$

If the pore pressure coefficient r_u is specified instead of piezometric surface coordinates, the outline describing the top of slope geometry is assumed as a hypothetical piezometric surface. The force pwp_{ig}^{ele} is calculated as the product of the unit weight of soil γ, pore pressure coefficient r_u, and the difference of y_{ig}^{ele} and y_{ps}.

$$pwp_{ig}^{ele} = r_u \times \gamma \times \left(y_{ps} - y_{ig}^{ele}\right) \tag{19}$$

The computed stresses are affected by the developed pore water pressure. To determine the effective stress components, it is required to modify the evaluated normal stress σ_{ig}^{ele} values at each gauss point; pwp_{ig}^{ele} is subtracted.

$$\sigma_{ig}'^{ele} = \sigma_{ig}^{ele} - pwp_{ig}^{ele} \tag{20}$$

Effect of Ponding

An illustrative diagram of a slope with impounded water is shown in Fig. 3. In order to model the effect of water, the gravity loads vector is modified by adding the water load. The additional load due to water is modeled as a normal stress with intensity varying from zero at the free surface to $\gamma_w(H_1 - H_W)$ at the toe for the submerged inclined portion of the soil slope. The water load applied on the foundation part is modeled as normal stresses with constant intensity equal to the product of the unit weight of water γ_w and height of standing water $(H_1 - H_W)$ above the foundation as shown in Fig. 2. All elements on the inclined surface as well as the horizontal surface of the foundation will be subjected to water load.

The procedure to calculate the equivalent nodal load vector due to impounded water is shown in Fig. 3. Figure 3a shows an arbitrary element '*i*' subjected to water loading. The water pressure intensity varies from p at node number 5 to q at node number 7. The trapezoidal pressure diagram shown in Fig. 3a is decomposed into triangular and rectangular pressure diagrams of water pressure intensity $q - p$ and p, respectively, as shown in Fig. 3b. The individual pressure diagrams are shown in Fig. 3c. Further, weight coefficients taken from Smith et al. [25] are used to convert these pressure diagrams into equivalent point loads as shown in Fig. 3d. Thereafter, these point loads are further resolved into horizontal and vertical components in order to determine equivalent nodal loads in respective directions as shown in Fig. 3e.

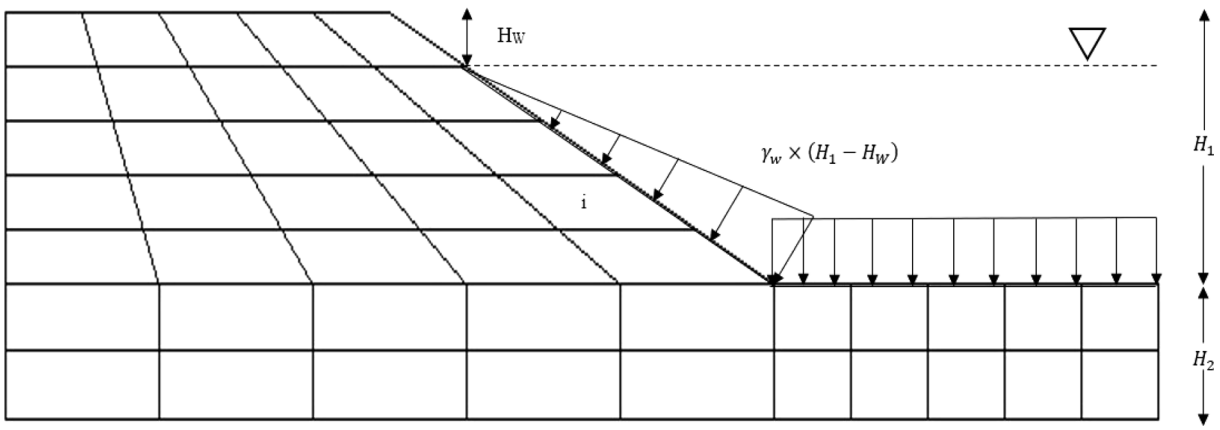

Fig. 2 Normal stresses equivalent to water loading

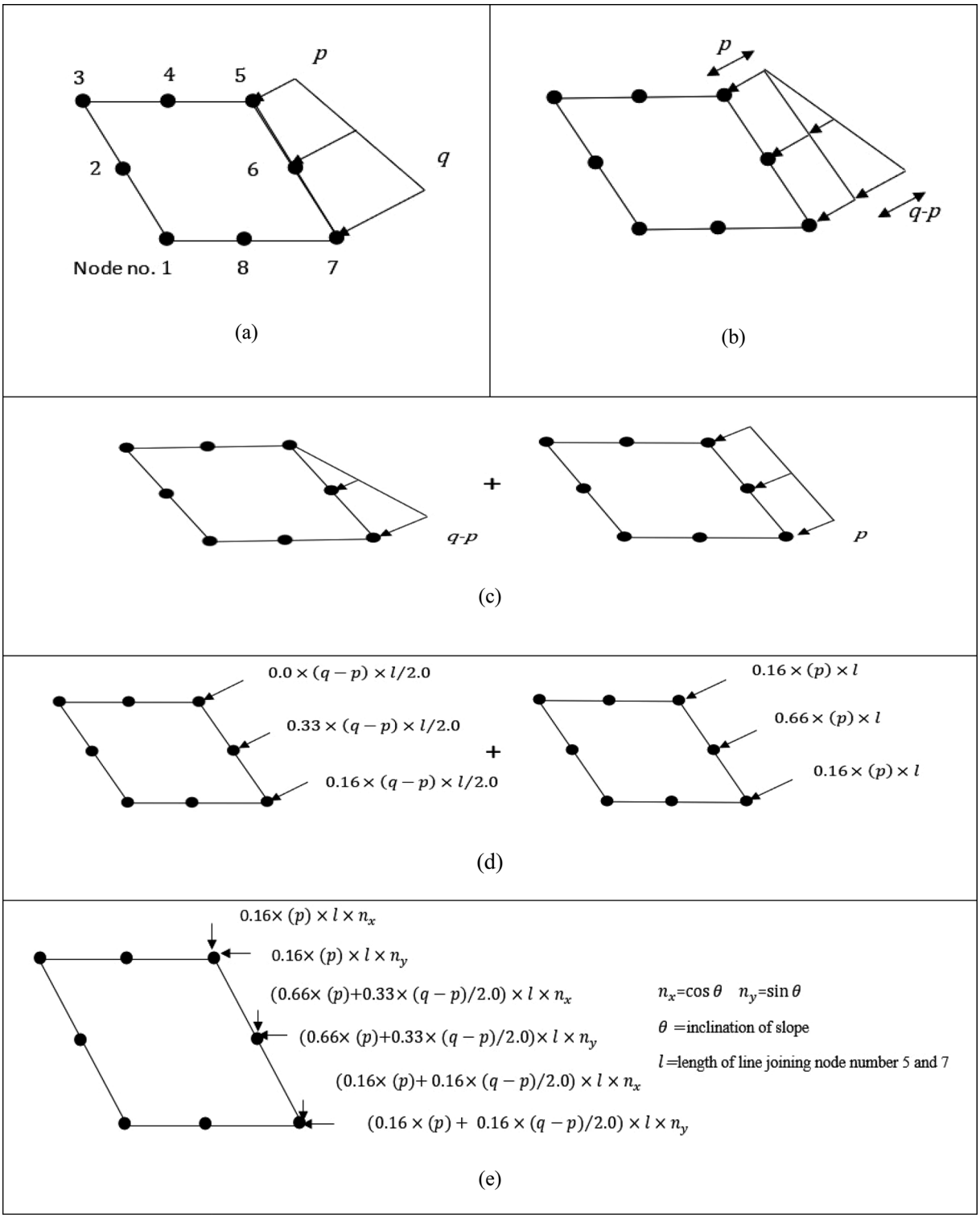

Fig. 3 **a** Element *i* with varying water pressure intensity. **b** Trapezoidal water load as sum of rectangular and triangular load. **c** Decomposed trapezoidal load. **d** Equivalent point loads. **e** Resolved equivalent nodal loads in respective direction

Equivalent Viscoplastic Strain

Identification of the zones that experience severe strain can be helpful in locating the failure surface of the slope. In this regard, equivalent viscoplastic strain can be used as an appropriate scalar quantity to represent the total viscoplastic strain at a point. Equivalent viscoplastic strain is a scalar measure of the plastic deformation experienced by the material in case of an arbitrary loading procedure. It is basically used as a measure for simulating strain softening phenomenon that is normally observed in soil. The expression for calculation of equivalent viscoplastic strain $\left(\varepsilon_{eq}^{vp}\right)$ as per Cook [32] is given as:

$$\varepsilon_{eq}^{vp}=\frac{\sqrt{2}}{3}\left[\left(\varepsilon_{x}^{vp}-\varepsilon_{y}^{vp}\right)^{2}+\left(\varepsilon_{y}^{vp}-\varepsilon_{z}^{vp}\right)^{2}+\left(\varepsilon_{z}^{vp}-\varepsilon_{x}^{vp}\right)^{2}+\frac{3}{2}\left\{\left(\gamma_{xy}^{vp}\right)^{2}+\left(\gamma_{yz}^{vp}\right)^{2}+\left(\gamma_{zx}^{vp}\right)^{2}\right\}\right]^{1/2} \tag{21}$$

Local Smoothing

In order to facilitate the generation of contour plots, least square interpolation procedure called local smoothing is made use of. Hinton and Campbell [33] proposed this idea. The parameters such as equivalent viscoplastic strain ε_{eq}^{vp}, Mohr–Coulomb failure function f_{mc}, and pore water pressure are first calculated at the gauss points and then they are transformed to equivalent nodal values using local smoothing technique. Further, contour plots are generated using nodal coordinates and the values of equivalent viscoplastic strains at nodes.

Results and Discussion

To put the proposed elastoviscoplastic finite element model to test and to check its applicability to numerous stability problems encountered in the field, a few slope stability problems have been taken from the literature. These slope stability problems have been thoroughly analyzed using other methods such as limit equilibrium method, limit analysis. The example problems investigated in the forthcoming section have been selected in such a way so that they represent varied loading conditions involving impounded water loads, seismic forces, etc. Also, slopes with weak soft layers and slopes with berms have been analyzed using the strength reduction technique discussed above. Fortran codes have been developed by making suitable alteration to the program 6.4 [25] to analyze all the above-mentioned problems. The program 6.4 developed by Smith et al. [25] has been modified to include the effects of pore water pressure, reservoir loading, seismic loading, and complex domains such as staged embankments.

Example 1 Homogeneous soil slope with ponded water.

For the purpose of validation of the results obtained using the current FEM-SRT-based model, an example problem has been taken from Donald and Giam [34]. The slope geometry of the example problem is shown in Fig. 4. The problem consists of a homogeneous soil slope of a height $H_1 = 10.0$ m. The material properties of the soil slope under consideration, namely c', $\phi'°$, γ take values equal to 11.0 kPa, 28.0°, and 20.0 kN/m^3, respectively. In order to perform slope stability analysis for the given geometry, an optimum mesh size should be selected. Sensitivity analysis is performed to determine the optimum mesh size. The discretized mesh consists of 1500 eight-nodded elements and 4701 nodes as shown in Fig. 5. For the considered slope geometry, two cases are considered. In the first case, the

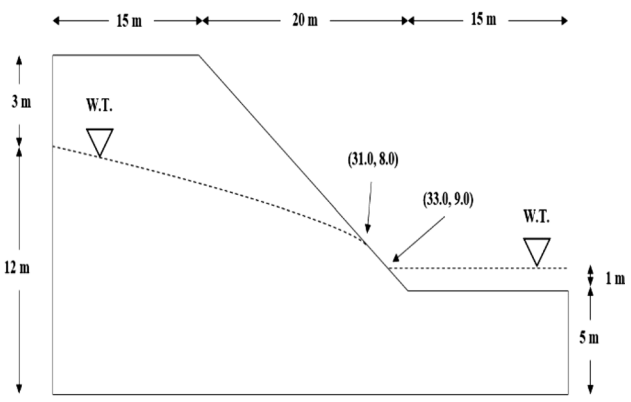

Fig. 4 Homogeneous soil slope with ponded water

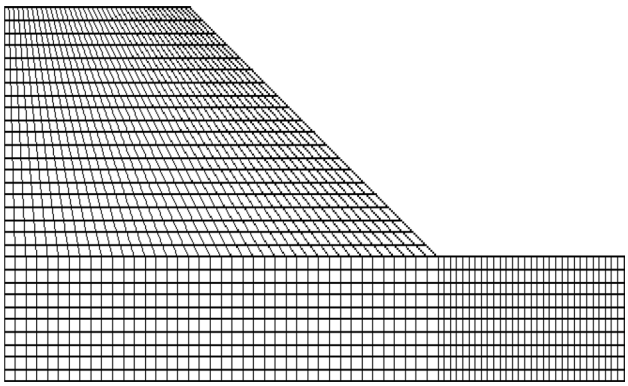

Fig. 5 Finite element mesh for the soil slope geometry shown in Fig. 4

Table 2 Comparison of results (F_S)

SLOPE/W				Current study
Bishop	Janbu	Morgenstern price	Spencer	
1.842	1.704	1.837	1.837	1.78

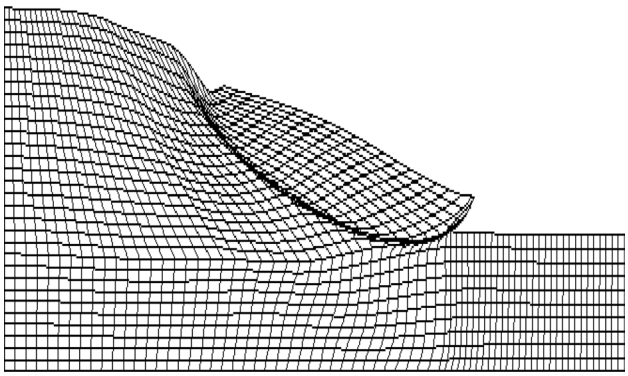

Fig. 6 Deformed mesh corresponding to non-convergent solution with $F_S = 1.78$

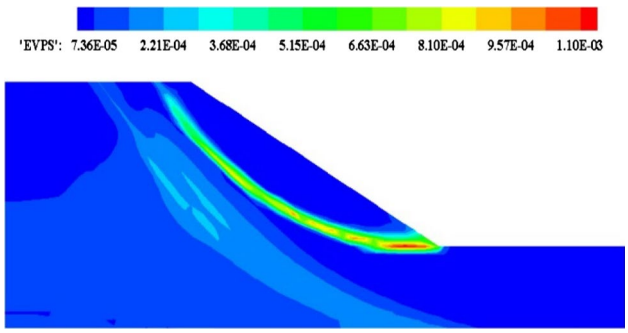

Fig. 7 Equivalent viscoplastic strain contours (Case 1)

effect of impounded water has not been taken into consideration i.e., dry conditions prevail and in the second case, the effect of pore water pressure and standing water load is taken into consideration.

Case 1: The current FEM-SRT model checks the stability of the considered slope geometry against a series of trial SRF values. For the trial SRF value equal to 1.775, the algorithm converged to equilibrium within the specified number of maximum iterations, while for SRF value equal to 1.78, the algorithm fails to converge within the specified number of maximum iterations. This indicates that the trial *SRF* value of 1.78 is the desired value of the factor of safety F_S. Table 2 shows the comparison of F_S. From the deformed mesh shown in Fig. 6, it is observed that the failure is essentially of toe type. The equivalent viscoplastic strain responsible for failure is shown in Fig. 7. From Fig. 7, it is observed that large values of $\boldsymbol{\varepsilon}_{\mathbf{eq}}^{\mathbf{vp}}$ are developed near the toe. From the deformed mesh shown in Fig. 6, it is observed that zones of failure extend from the crest of the slope up to the toe, thereby inducing a failure mechanism. Figure 7 shows that the higher values of equivalent viscoplastic strains occurred in the zones of higher displacement as observed from the deformed mesh shown in Fig. 6. Figure 8 shows the plot of the failure function f_{mc}. The locations with $f_{mc} = 0.0$ indicate yielding. These yielded regions are further represented by yellow-colored zones extending from the top of the slope up to the toe. The yielded regions are clearly indicative of the fact that the stresses in the soil are in a state of yield along the failure surface.

Case 2: In this case, the effect of pore water pressure and the standing water load has been taken into consideration. The finite element mesh shown in Fig. 5 is used for slope stability analysis. Using the current FEM-SRT-based model, corresponding to the trial value of SRF = 1.444 the algorithm converged to equilibrium within the specified number of maximum iterations. Further corresponding to

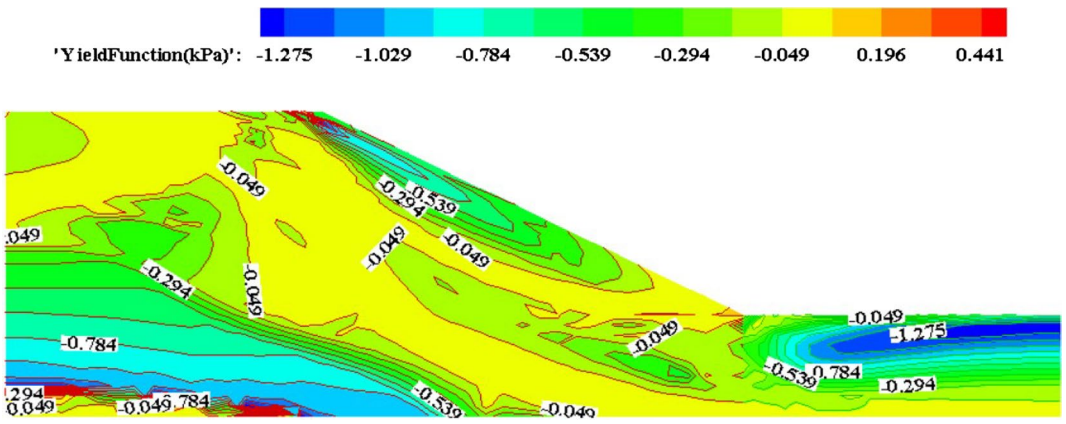

Fig. 8 Contours of f_{mc} corresponding to non-convergent solution with $F_S = 1.78$

Table 3 Comparison of results (F_E)

Donald and Giam [34]	Slide2 slope verification manual			Deep EX slope stability analysis manual			Current study
1.53	Bishop	Spencer	Janbu corrected	Bishop	Spencer	Generalized limit equilibrium	1.45
	1.498	1.5	1.457	1.496	1.433	1.429	

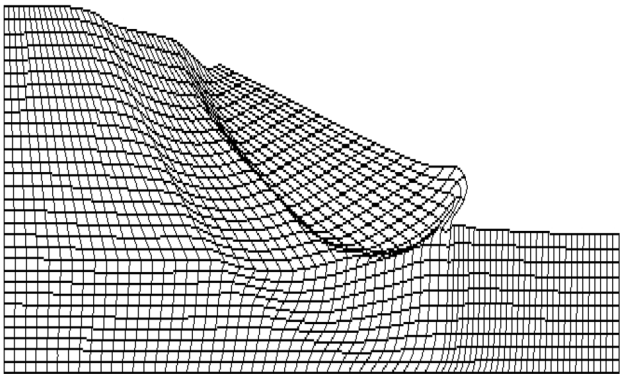

Fig. 9 Deformed mesh corresponding to non-convergent solution with $F_S = 1.45$

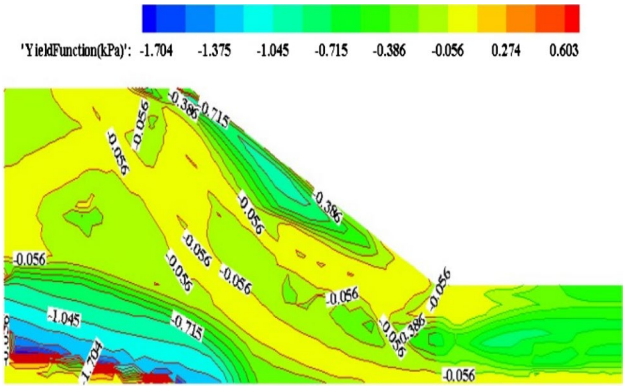

Fig. 12 Contours of f_{mc} corresponding to non-convergent solution with $F_S = 1.45$

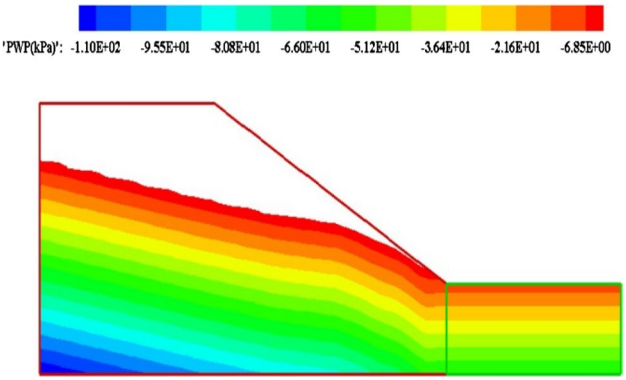

Fig. 10 Pore water pressure contour plot (Case 2)

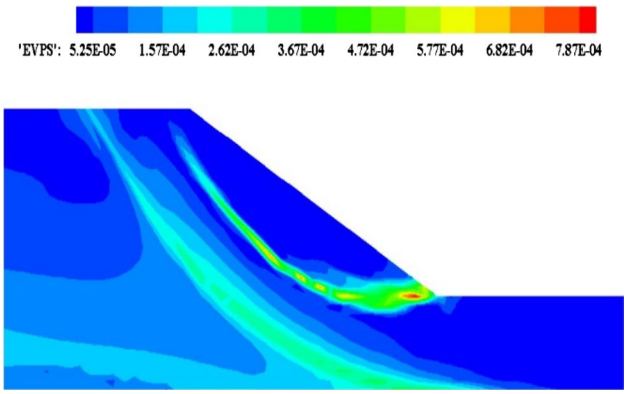

Fig. 11 Equivalent viscoplastic strain contours (Case 2)

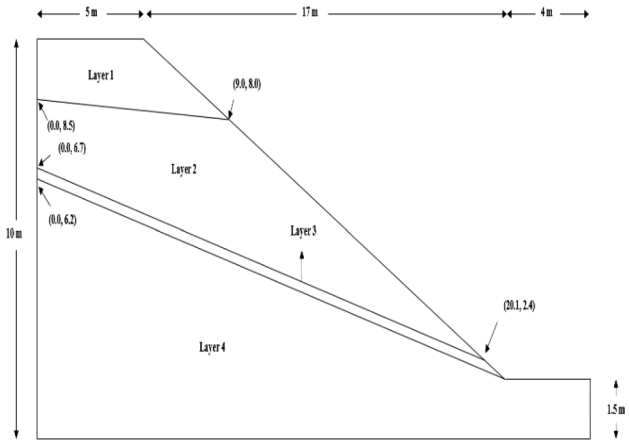

Fig. 13 Layered soil slope with an inclined weak layer

Table 4 Material properties for layered soil slope (Example 2)

Layer	c'(kPa)	$\phi'°$	γ (kN/m^3)
1	15.0	20.0	18.62
2	17.0	21.0	18.62
3	5.0	10.0	18.62
4	35.0	28.0	18.62

the next trial value of SRF = 1.45, the algorithm fails to establish global equilibrium, thereby indicating that the trial SRF = 1.45 is the desired value of F_S. Table 3 shows the comparison of F_S. The deformed mesh corresponding

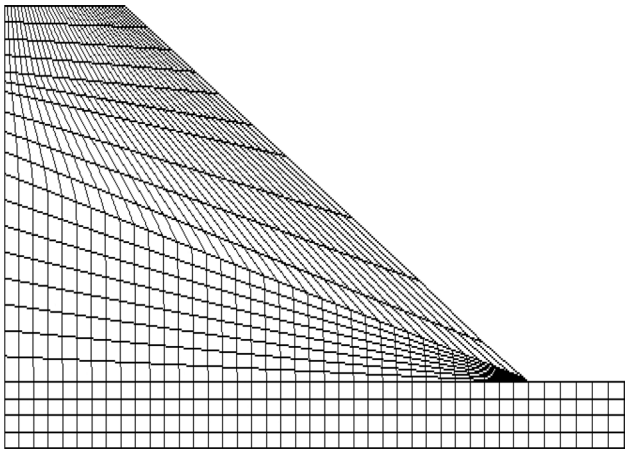

Fig. 14 Finite element mesh for slope geometry (Example 2)

Table 5 Comparison of results (F_S)

Cheng et al. [37],	Liu et al. [36]	Navneet Himanshu et al. [35]	Current study
1.13	1.111	1.10	1.13

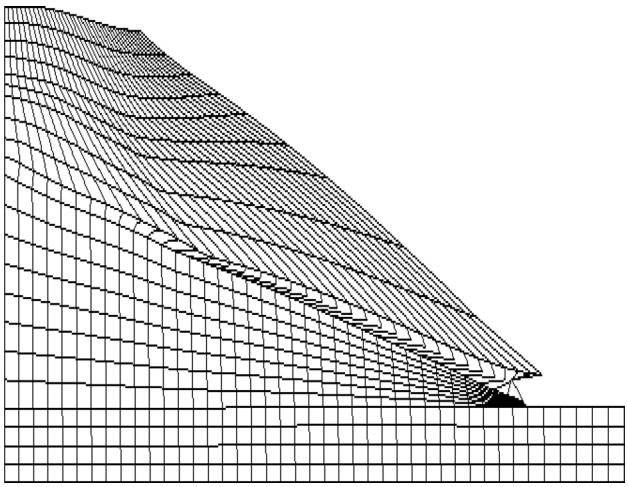

Fig. 15 Deformed mesh corresponding to non-convergent solution with $F_S = 1.13$

to non-convergent solution at $F_S = 1.45$ is shown in Fig. 9. The failure observed is essentially of toe type with a reduced value of F_S. Pore pressure distribution is shown in Fig. 10. From Fig. 10, it is observed that the pore water pressure gradually decreases from the left face up to the toe. It then becomes constant up to the right face. It is again seen that high values of $\boldsymbol{\varepsilon}_{\mathbf{eq}}^{\mathbf{vp}}$ occur near the locations

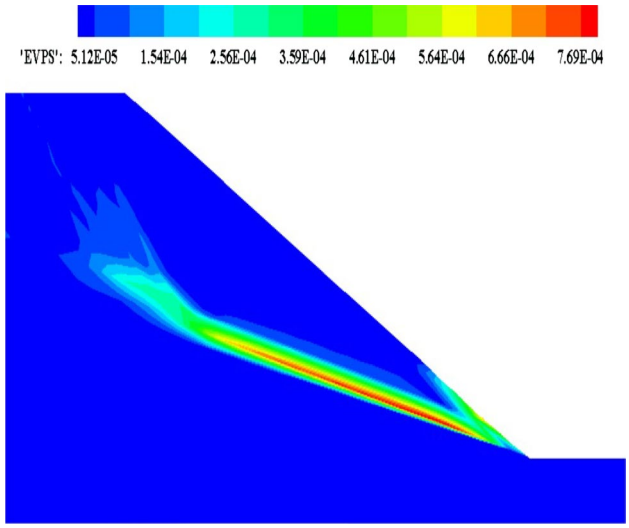

Fig. 16 Equivalent viscoplastic strain contours (Example 2)

of higher displacements as seen in Figs. 9 and 11. The equivalent viscoplastic strain is shown in Fig. 11. From Fig. 11, it is observed that large values of $\boldsymbol{\varepsilon}_{\mathbf{eq}}^{\mathbf{vp}}$ are developed near the toe. The magnitude of the $\boldsymbol{\varepsilon}_{\mathbf{eq}}^{\mathbf{vp}}$ is somewhat less than that corresponding to dry conditions. Figure 12 shows the plot of the failure function f_{mc}. Yielding regions are represented by yellow-colored zones extending from the top of the slope up to the toe.

Example 2 Layered soil slope with an inclined weak layer.

Example 2 shown in Fig. 13 has been taken from the works of Himanshu et al. [35]. The considered slope geometry has also been evaluated by many researchers [27, 36]. The soil slope shown in Fig. 13 consists of four different layers of soil. The material properties of each layer are mentioned in Table 4.

As per the mesh sensitivity analysis, 816 elements are sufficient for the considered slope geometry as shown in Fig. 14. For the slope geometry shown in Fig. 13, global equilibrium fails to establish corresponding to a trial SRF value equal to 1.13. This trial SRF value is the desired value of F_S. The values obtained by the current FEM-SRT-based model are in close comparison with the values obtained by other researchers as shown in Table 5. The deformed mesh corresponding to the non-convergent solution at $F_S = 1.13$ is shown in Fig. 15. From the deformed mesh, it is observed that the mechanism of failure was concentrated along the

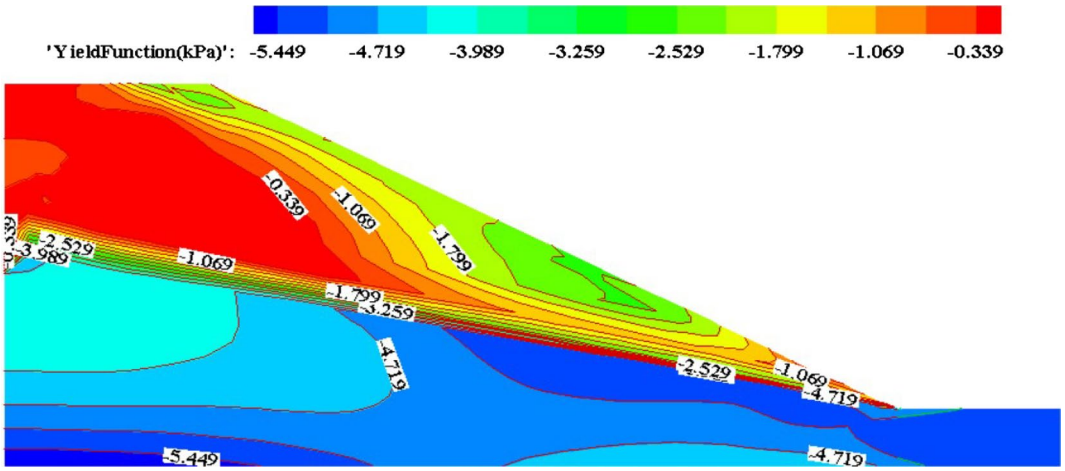

Fig. 17 Contours of f_{mc} corresponding to non-convergent solution with $F_S = 1.13$

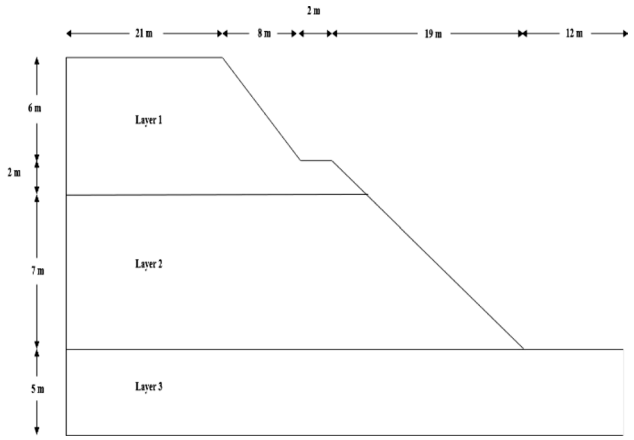

Fig. 18 Ireland congress street cut

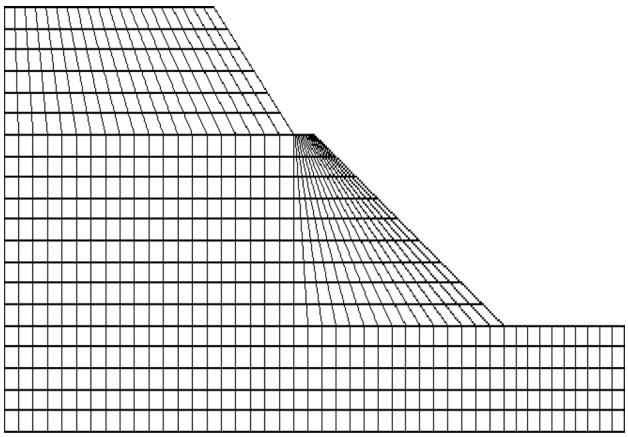

Fig. 19 Finite element mesh (Example 3)

Table 6 Material properties for staged embankment (Fig. 18)

Layer	c'(kPa)	$\phi'°$	γ (kN/m^3)
1	3.0	30.0	21.0
2	22.0	11.0	22.0
3	25.0	20.0	22.0

Table 7 Comparison of results (F_S)

Ireland [46]	Oka and Wu[39]	Chowdhury and Xu [40]	Matthews et al. [38]	Current study
1.11	1.12	1.117	1.20	1.12

weak layer. Zones of failure remain confined to the regions above the toe of the slope, thereby forming a shallow failure mechanism. The equivalent viscoplastic strain is shown in Fig. 16. From Fig. 16, it is observed that high $\boldsymbol{\varepsilon}_{\mathbf{eq}}^{\mathbf{vp}}$ is developed along the soil layer possessing inferior strength properties. Figure 17 shows the plot of the failure function f_{mc}. From Fig. 17 it is observed that yielding regions are confined to the soil layer having inferior material properties.

Example 3 Ireland congress street cut.

Example 3 shown in Fig. 18 has been adopted from Matthews et al. [38]. This example is a slightly modified version of the famous congress street open cut in Chicago. This problem has been earlier studied by many researchers such as Oka and Wu [39], Chowdhury and Xu [40]. The soil slope shown in Fig. 18 consists of 3 different layers of soil. Layer 1 extends up to a depth of 8.0 m, layer 2 extends up to a depth of 15.0 m, and layer 3 extends up to 20.0 m. Table 6 shows the material properties of different layers of the slope.

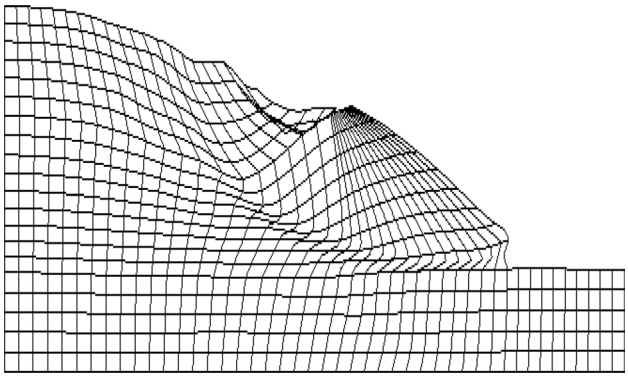

Fig. 20 Deformed mesh corresponding to non-convergent solution with $F_S = 1.12$

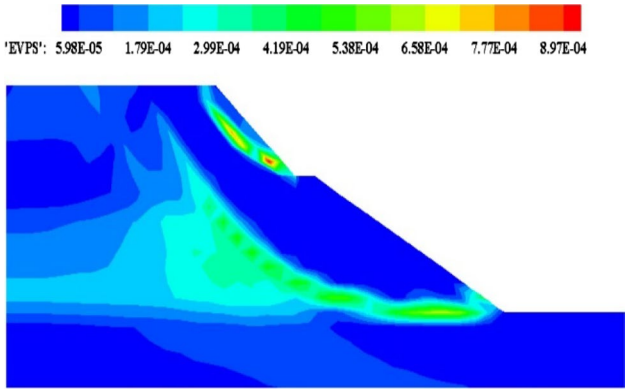

Fig. 21 Equivalent viscoplastic strain contours (Case 1)

As per the mesh sensitivity analysis, 660 elements are adopted for the considered slope geometry as shown in Fig. 19. For the considered slope geometry, three cases are considered. In the first case, the soil slope is not subjected to any of the destabilizing forces. In the second case, the soil slope is subjected to earthquake loads in the horizontal direction, while in the third case, the soil slope is subjected to earthquake loads along both horizontal and vertical directions.

Case 1: For the heterogeneous slope geometry shown in Fig. 18, the non-convergence of the algorithm within the specified displacement tolerance and plastic iteration limit occurs at $SRF = 1.12$. This SRF value is the desired value of F_S. The values obtained by the current FEM-SRT-based model are in close comparison with the values obtained by other researchers as shown in Table 7. The deformed mesh corresponding to non-convergent solution at $F_S = 1.12$ is shown in Fig. 20. From Fig. 20, the existence of a conflicting failure mechanism is observed. Conflicting mechanisms refer to one or more failure mechanisms occurring simultaneously within the slope profile. It is observed that two failure mechanisms are developing simultaneously, one along the top sloping part coming out at the top toe, while another coming out at the bottom toe along the bottom slope, thereby forming conflicting failure mechanisms. The contour plot for the effective viscoplastic strain is shown in Fig. 21. From Fig. 21, it is observed that large values occurred near the toe for the first inclined part as compared to the second inclined part of the staged embankment. Also, these larger values occur in the zones of higher displacements as observed in Fig. 20 and 21. Figure 22 shows the plot of the failure function f_{mc}. Yielding regions are confined near the toe regions of two sloping portions of the staged embankment. Therefore, the generation of zones of multiple failure regions is displayed in Fig. 20 by the color bands depicting equivalent viscoplastic strains as well as the yield functions. Since the FEM-SRT method induces slope failure based on developed stresses, the generation of multiple failure surfaces is manifested by this method. The other slope analysis methods such as limit equilibrium methods[41–44] and limit

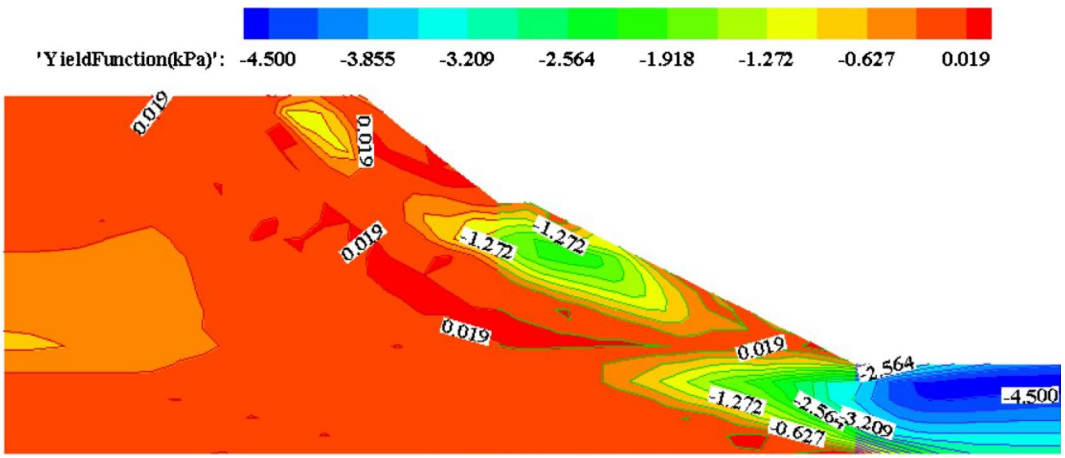

Fig. 22 Contours of f_{mc} corresponding to non-convergent solution with $F_S = 1.12$

Table 8 Comparison of results (F_S)

SLOPE/W				Current study
Bishop	Janbu	Morgenstern price	Spencer	
0.939	0.855	0.929	0.927	0.89

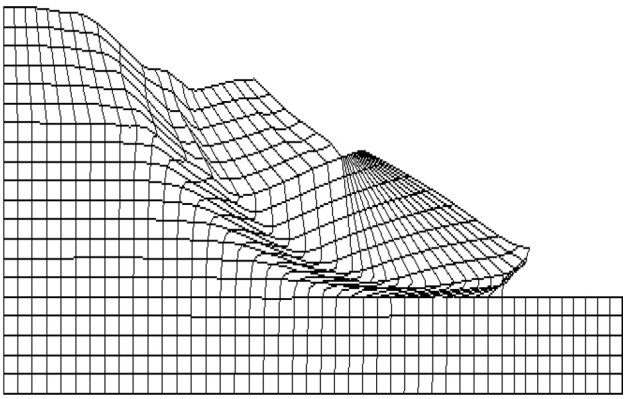

Fig. 23 Deformed mesh corresponding to non-convergent solution with $F_S = 0.89$

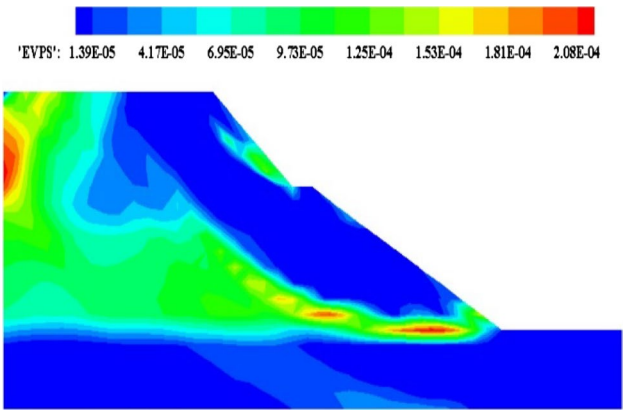

Fig. 24 Equivalent viscoplastic strain contours (Case 2)

analysis methods[3, 4, 45] only report the critical failure surface and hence are unable to show the generations of multiple failure regions, if there are any.

Case 2: For this instance, a k_h value of 0.10 to consider earthquake effects is assumed. The cross section of slope (Fig. 16) when analyzed using the current FEM-SRT-based model returned a F_S value of 0.89. Table 8 shows the comparison of F_S determined using different methods. The deformed mesh corresponding to the non-convergent solution at $F_S = 0.89$ is shown in Fig. 23. From Fig. 23, it is observed that the failure zones do not reach the foundation part, thereby forming a shallow failure mechanism. The contour plot for the equivalent viscoplastic strain is shown in Fig. 24. From Fig. 24, it is observed that a larger $\boldsymbol{\varepsilon}_{\mathbf{eq}}^{\mathbf{vp}}$ developed near the toe of the second inclined part of the staged embankment. The value of $\boldsymbol{\varepsilon}_{\mathbf{eq}}^{\mathbf{vp}}$ is found to be greater as compared to case 1 and occurred in the zones of larger displacements. Figure 25 shows the plot of the failure function f_{mc}. Non-negative values of f_{mc} are observed near the toes of the two sloping portions of the staged embankment.

Case 3: For this instance, k_h remains unchanged from the previous case, while a k_v value equal to half of k_h is adopted. The cross section of slope (Fig. 18) when analyzed using the current FEM-SRT-based model returned a F_S value of 0.88. Table 9 shows the comparison of F_S determined using different methods. The deformed mesh corresponding to non-convergent solution at $F_S = 0.88$ is shown in Fig. 26. Shallow failure mechanism like case 2 occurred in the current case also. The contour plot for the equivalent viscoplastic strain is shown in Fig. 27. From Fig. 27, it is observed that the behavior is similar to case 2. The magnitude of $\boldsymbol{\varepsilon}_{\mathbf{eq}}^{\mathbf{vp}}$ is found to be smaller as compared to the above two cases. Figure 28 shows the plot of the failure function f_{mc}. Non-negative values of failure function are observed near the sloping portion of the staged embankment.

Conclusions

The present study discusses the development of a finite element program based on the strength reduction technique. Mohr–Coulomb failure criteria have been adopted to represent the stress–strain response of the soil material. Different problems including a homogenous slope subjected to external water loading, a slope with inclined weak layer, and a slope with berms subjected to horizontal and vertical earthquake loading have been analyzed to establish the validity of the results. The following conclusions are summarized as follows:

(a) From the different examples considered in the current study, it is observed that the value of the factor of safety determined using the current slope stability model lies closer to that obtained by other researchers. Furthermore, the FS values have been compared with SLOPE/W results which are also seen to match quite well the results obtained using FEM-SRT methods.
(b) Failure zone extends from the crest of the slope up to the toe of the slope in most of the cases as indicated by the deformed mesh.
(c) The plots of equivalent viscoplastic strains show that higher values of strains occur in the zones of larger

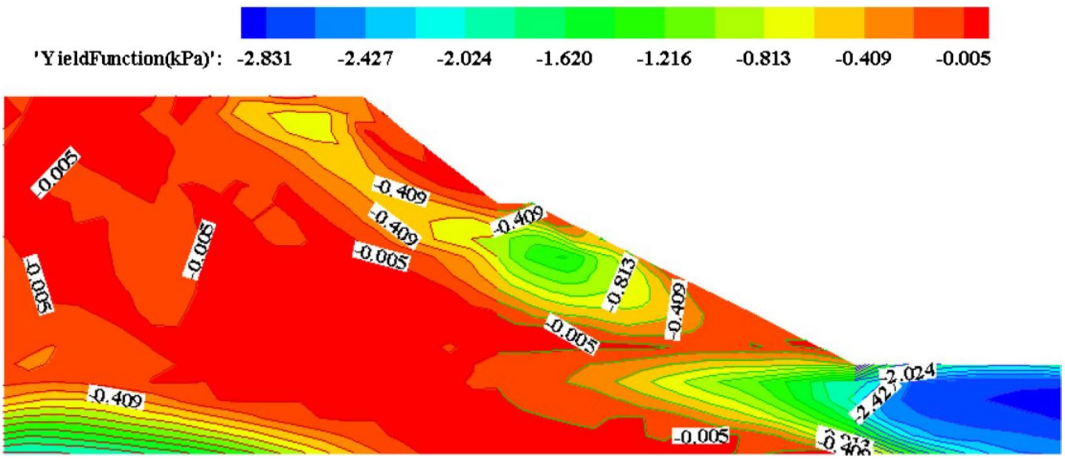

Fig. 25 Contours of f_{mc} corresponding to non-convergent solution with $F_S = 0.89$

Table 9 Comparison of results (F_S)

SLOPE/W				Current study
Bishop	Janbu	Morgenstern price	Spencer	
0.931	0.848	0.920	0.919	0.88

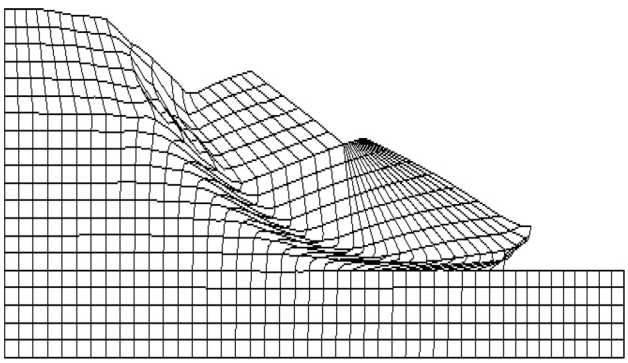

Fig. 26 Deformed mesh corresponding to non-convergent solution with $F_S = 0.88$

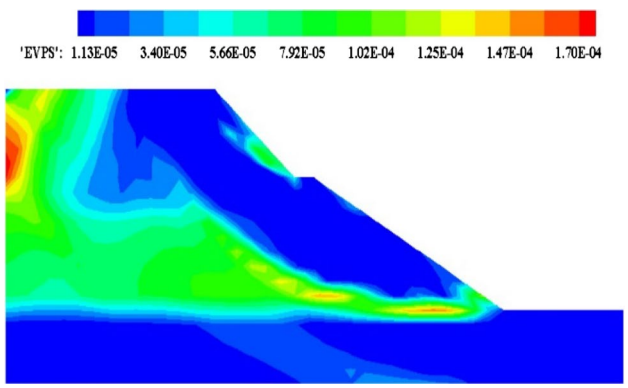

Fig. 27 Equivalent viscoplastic strain contours (Case 3)

displacements, and this fact can also be verified from the deformed mesh structure.

(d) Contour plots of yield function are in good agreement with the plot of deformed mesh and equivalent viscoplastic strains with yielding taking place in the zones of larger displacement and higher equivalent viscoplastic strains. The yield function approaches zero value near the failure surface indicating the yielding of the material.

(e) A decrease in the value of the factor of safety is observed in case the soil slope is subjected to pore water pressure and reservoir loading with reduced values of equivalent viscoplastic strains compared to the situations when pore water pressure and reservoir loadings are absent.

(f) If seismic loading is applied, the factor of safety of the slope is observed to decrease. The corresponding equivalent viscoplastic strains and yield function plots show higher distress in the slope domain.

(g) The deformation profile of the mesh, equivalent viscoplastic strains, and yield function plots are helpful to visualize the response of the staged embankment at the time of failure.

(h) The FEM-SRT-based solution of stepped embankment manifests a very interesting phenomenon that multiple failure zones may develop at the time of failure as indicated by contour plots of equivalent viscoplastic strains and yield functions. Since the FEM-SRT-based slope analysis method induces slope failure based on developed stresses in the failure zones, such developments of multiple zones of failure are very much possible. Other slope analysis methods such as limit equilibrium and limit analysis methods cannot depict this phenomenon.

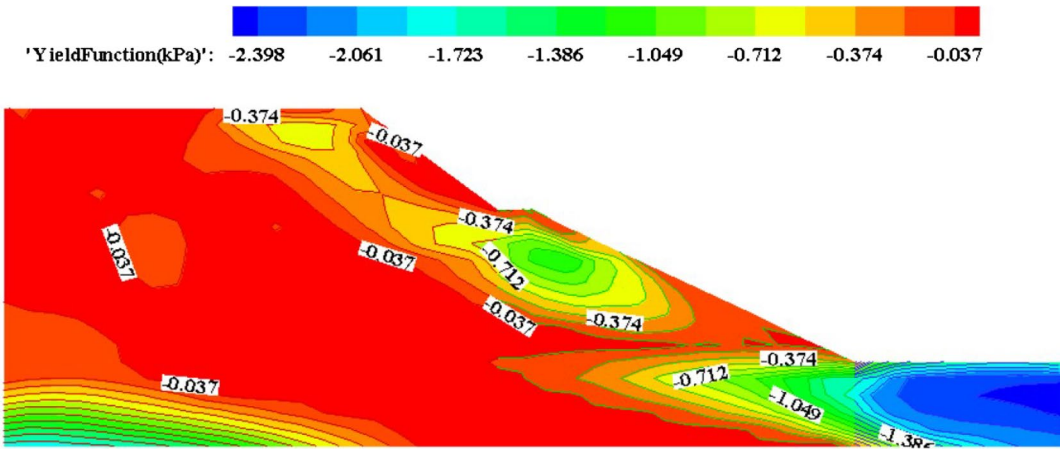

Fig. 28 Contours of f_{mc} corresponding to non-convergent solution with $F_S = 0.88$

Limitations, Future Scopes, and Practical Applications

The FEM-SRT-based slope stability program developed by the authors can analyze a soil slope against diverse loading conditions including reservoir water loading, seismic forces through the pseudo-static method, etc. It can also be used to analyze stepped embankments as well. The developed FEM-SRT-based slope stability program can be effectively used to study drawdown effects in reservoirs. Furthermore, rock slope analysis can also be performed if suitable constitutive models such as the Hoek–Brown failure criterion are incorporated into the program. The developed program can be extended for three-dimensional slope stability analysis. Also, the developed program can be modified to study the reinforced soil slope failure.

Data Availability All data will be made available on request.

Declarations

Conflict of interest The authors declare that they have no conflict of interest.

References

1. Nie X, Chen K, Zou D et al (2022) Slope stability analysis based on SBFEM and multistage polytree-based refinement algorithms. Comput Geotech 149:104861
2. Krahn J (2003) The 2001 RM hardy lecture: the limits of limit equilibrium analyses. Can Geotech J 40:643–660
3. Drucker DC, Prager W (1952) Soil mechanics and plastic analysis or limit design. Q Appl Math 10:157–165
4. Viratjandr C, Michalowski RL (2006) Limit analysis of submerged slopes subjected to water drawdown. Can Geotech J 43:802–814
5. Utili S (2013) Investigation by limit analysis on the stability of slopes with cracks. Geotechnique 63:140–154
6. Xu J, Li Y, Yang X (2018) Seismic and static 3D stability of two-stage slope considering joined influences of nonlinearity and dilatancy. KSCE J Civ Eng 22:3827–3836. https://doi.org/10.1007/s12205-018-0636-z
7. Huang W, Loveridge F, Satyanaga A (2022) Translational upper bound limit analysis of shallow landslides accounting for pore pressure effects. Comput Geotech 148:104841
8. Payan M, Fathipour H, Hosseini M et al (2022) Lower bound finite element limit analysis of geo-structures with non-associated flow rule. Comput Geotech 147:104803
9. Carrión M, Vargas EA, Velloso RQ, Farfan AD (2017) Slope stability analysis in 3D using numerical limit analysis (NLA) and elasto-plastic analysis (EPA). Geomech Geoengin 12:250–265
10. Zienkiewicz OC, Humpheson C, Lewis RW (1975) Associated and non-associated visco-plasticity and plasticity in soil mechanics. Geotechnique 25:671–689
11. Griffiths DV, Lane PA (1999) Slope stability analysis by finite elements. Geotechnique 49:387–403
12. Chugh AK (2003) On the boundary conditions in slope stability analysis. Int J Numer Anal methods Geomech 27:905–926
13. Cheng YM, Lansivaara T, Wei WB (2007) Two-dimensional slope stability analysis by limit equilibrium and strength reduction methods. Comput Geotech 34:137–150
14. Berilgen MM (2007) Investigation of stability of slopes under drawdown conditions. Comput Geotech 34:81–91. https://doi.org/10.1016/j.compgeo.2006.10.004
15. Zheng H, Sun G, Liu D (2009) A practical procedure for searching critical slip surfaces of slopes based on the strength reduction technique. Comput Geotech 36:1–5. https://doi.org/10.1016/j.compgeo.2008.06.002
16. Khosravi M, Leshchinsky D, Meehan CL, Khosravi A (2013) Stability analysis of seismically loaded slopes using finite element techniques. In: Geo-congress 2013: stability and performance of slopes and embankments III, pp 1310–1319
17. Lu L, Wang ZJ, Song ML, Arai K (2015) Stability analysis of slopes with ground water during earthquakes. Eng Geol 193:288–296. https://doi.org/10.1016/j.enggeo.2015.05.001

18. Chen X, Ren J, Liu J (2017) Analysis of slope stability and software development based on single-grid and two-grid finite element methods. Geotech Geol Eng 35:1369–1382
19. Tschuchnigg F, Schweiger HF, Sloan SW (2015) Slope stability analysis by means of finite element limit analysis and finite element strength reduction techniques. Part I: numerical studies considering non-associated plasticity. Comput Geotech 70:169–177
20. Dyson AP, Tolooiyan A (2018) Optimisation of strength reduction finite element method codes for slope stability analysis. Innov Infrastruct Solut 3:38
21. Meng QX, Wang HL, Xu WY et al (2019) Multiscale strength reduction method for heterogeneous slope using hierarchical FEM/DEM modeling. Comput Geotech 115:103164
22. Liu F (2020) Stability analysis of geotechnical slope based on strength reduction method. Geotech Geol Eng 38:3653–3665
23. Sun W, Wang G, Zhang L (2021) Slope stability analysis by strength reduction method based on average residual displacement increment criterion. Bull Eng Geol Environ 80:4367–4378
24. Mebrahtu TK, Heinze T, Wohnlich S, Alber M (2022) Slope stability analysis of deep-seated landslides using limit equilibrium and finite element methods in Debre Sina area. Ethiopia Bull Eng Geol Environ 81:403
25. Smith IM, Griffiths DV, Margetts L (2013) Programming the finite element method. Wiley, New York
26. SNITBHAN AM, Chen WF (1976) Finite element analysis of large deformation in slopes. In: Proceedings of the international symposium on numerical methods in geomechanics
27. Duncan JM, Dunlop P (1969) Slopes in stiff-fissured clays and shales. J Soil Mech Found Div 95:467–492
28. Zienkiewicz OC, Morice PB (1971) The finite element method in engineering science. McGraw-hill, London
29. Soranzo E, Guardiani C, Chen Y, Wang Y, Wu W (2023) Convolutional neural networks prediction of the factor of safety of random layered slopes by the strength reduction method. Acta Geotechnica 18(6):3391–3402
30. Heister T, Rebholz LG, Xue F (2019) Numerical analysis: an introduction. Walter de Gruyter GmbH & Co KG
31. Tanakan S (2013) A new algorithm of modified bisection method for nonlinear equation. Appl Math Sci 7:6107–6114
32. Cook RD (2007) Concepts and applications of finite element analysis. Wiley, New York
33. Hinton E, Campbell J (1974) Local and global smoothing of discontinuous finite element functions using a least squares method. Int J Numer Methods Eng 8:461–480
34. Donald IB, Giam PSK (1989) Example problems for testing soil slope stability programs (No. 8/1989). Monash University, Victoria Australia
35. Himanshu N, Burman A, Kumar V (2021) Numerical study of optimal location of non-circular segmented failure surface in soil slope with weak soil layer. Int J Appl Metaheur Comput 12:111–141
36. Liu S, Su Z, Li M, Shao L (2020) Slope stability analysis using elastic finite element stress fields. Eng Geol 273:105673
37. Cheng YM, Li L, Chi SC (2007) Performance studies on six heuristic global optimization methods in the location of critical slip surface. Comput Geotech 34:462–484
38. Matthews C, Farook Z, Helm P (2014) Slope stability analysis–limit equilibrium or the finite element method. Gr Eng 48:22–28
39. Oka Y, Wu TH (1990) System reliability of slope stability. J Geotech Eng 116:1185–1189
40. Chowdhury RN, Xu DW (1995) Geotechnical system reliability of slopes. Reliab Eng Syst Saf 47:141–151
41. Bishop AW (1955) The use of the slip circle in the stability analysis of slopes. Geotechnique 5:7–17
42. Janbu N (1973) Slope stability computations–Embankment–Dam Engineering. Casagrande Volume. Wiley, New York, pp 47–86
43. Morgenstern NR, Price VE (1965) The analysis of the stability of general slip surfaces. Geotechnique 15:79–93
44. Fredlund DG, Krahn J (1977) Comparison of slope stability methods of analysis. Can Geotech J 14:429–439
45. Chen WF (ed) (2013) Limit analysis and soil plasticity. Elsevier
46. Ireland HO (1954) Stability analysis of the Congress Street open cut in Chicago. Geotechnique 4:163–168